Note S1. Main glove

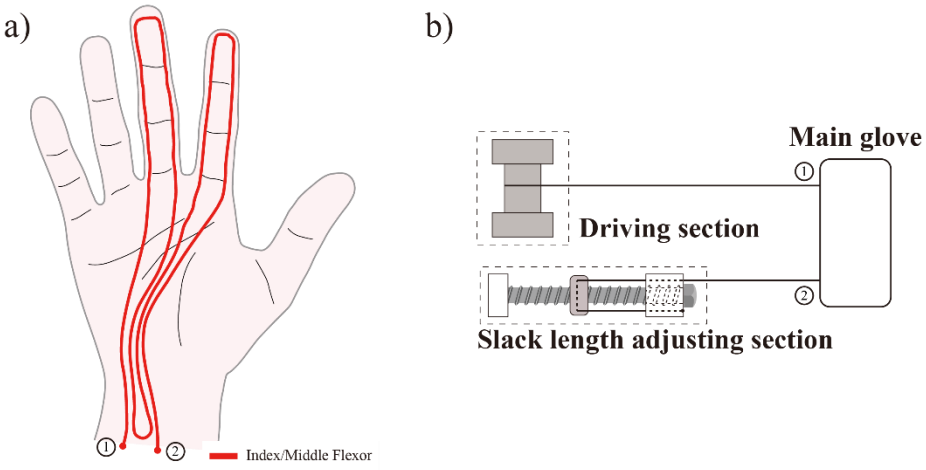

Figure. S1 A routing of the flexor. (a) Routing of the flexor in the main glove. The flexor originates from the spool (①) and ends at slack length adjusting section (②). (b) Overview of flexor in the system.

We used two nickel-titanium wires (Φ0.6 mm for the index finger and Φ0.8 mm for the middle finger) as passive extensors, relying on their high bending stiffness for passive extension, thus reducing axial force on the fingers and improving overall comfort [1]. As indicated by the difference in diameters, the passive extensors in each finger have different bending stiffness. Since the flexor originates from the spool and passes through tendon routings in the main glove and ends at the slack length adjusting section (Fig. S1(a), (b)), friction between the tendon and the routing causes the tension to decrease from ① to ② in Fig. S1. Due to the tension difference, the middle finger bends first. To move the fingers at the same time, we used a thicker passive extensor for the middle finger, which needs higher tension to flex the middle finger and delays the middle finger flexion timing. When flexor tension decreases, these elements extend the index and middle fingers, establishing an open hand as the neutral posture. Two nitinol wires were inserted in Teflon tubes, where previous extensors (of EGP II) passed through. One end of the nitinol wire is fixed in a thimble hole, while the other is free inside the Teflon tube. This setup allows the wire to slide out of the tube when the finger flexes.

In addition to the passive extensors, the palm strap's original magnetic anchoring is replaced with a buckle-type anchoring method. This is because the tension of the thumb encloser (Fig. 3(b) in the manuscript) causes the glove to fall apart from the hand.

Reference

1. P. Tran, S. Jeong, S. L. Wolf, and J. P. Desai, “Patient-specific, voice-controlled, robotic flexotendon glove-ii system for spinal cord injury,” IEEE Robotics and Automation Letters, vol. 5, no. 2, pp. 898–905, 2020.

Note S2. Slack-enabling mechanism to prevent malfunctioning.

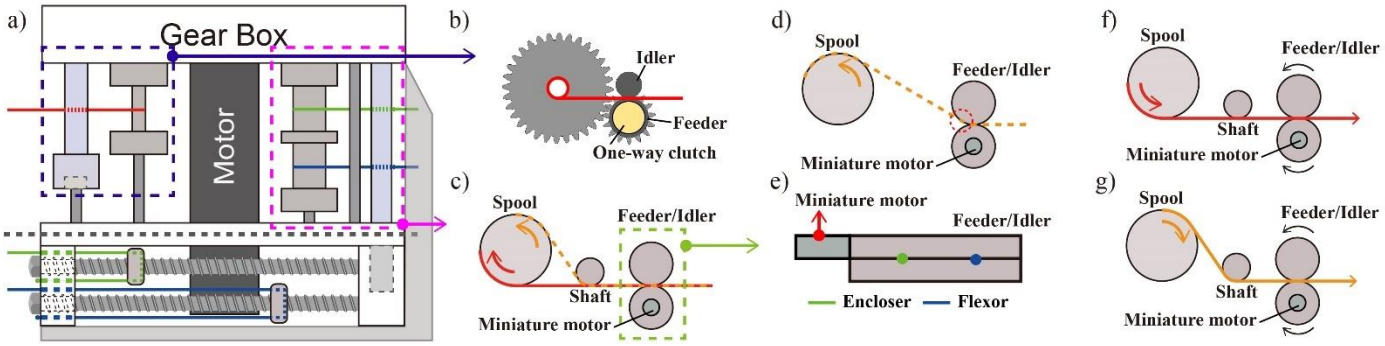

Figure. S2 Design of the slack-based sequential actuator. (a) Driving section of the actuator. (b) Slack-enabling mechanism for opposer. The feeder is mechanically connected to the spool via gears. A one-way clutch is embedded in the feeder to transfer power from the motor to the feeder only in one direction for tendon release [1]. (c) Location of additional shaft preventing damage to the feeder and idler. (d) Possible failure when the shaft is not added to the slack-enabling mechanism for the flexor and the encloser. The tendon can damage the idler in a red dotted circle. (e) Miniature motor, feeder, and idler for slack-enabling mechanism for the flexor and the encloser. (f) Slack-enabling mechanism when the spool for the flexor and the encloser rotates counterclockwise. (g) Slack-enabling mechanism when the spool for the flexor and the encloser rotates clockwise.

Since we utilized the slack for the SSM, a slack-enabling mechanism is used to prevent system failure in both spools. The previously proposed method [1] is used for the opposer, where slack-enabling occurs only in one direction of the spool rotation (Fig. S2(b)). Since the flexor and the encloser are pulled in both clockwise and counterclockwise rotations (Fig. S2(c)), the release of the tendons also occurs in both rotations. Therefore, a miniature motor rotates the feeder to continuously push the tendon outwards during actuation (Fig. S2(e), (f), (g)). Additionally, a shaft is inserted between spools to prevent damage to the feeder/idler by the tendon and enables tendons to be tangential to both spools (Fig. S2(c)). Without the shaft, the tension of the tendon can tear the idler while the spool rotates counterclockwise (Fig. S2(d)).

Reference

1. H. In, U. Jeong, H. Lee, and K.-J. Cho, “A novel slack-enabling tendon drive that improves efficiency, size, and safety in soft wearable robots,” IEEE/ASME Transactions on Mechatronics, vol. 22, no. 1, pp. 59–70, 2016.

Note S3. Motion Sequence for Grasping Strategy

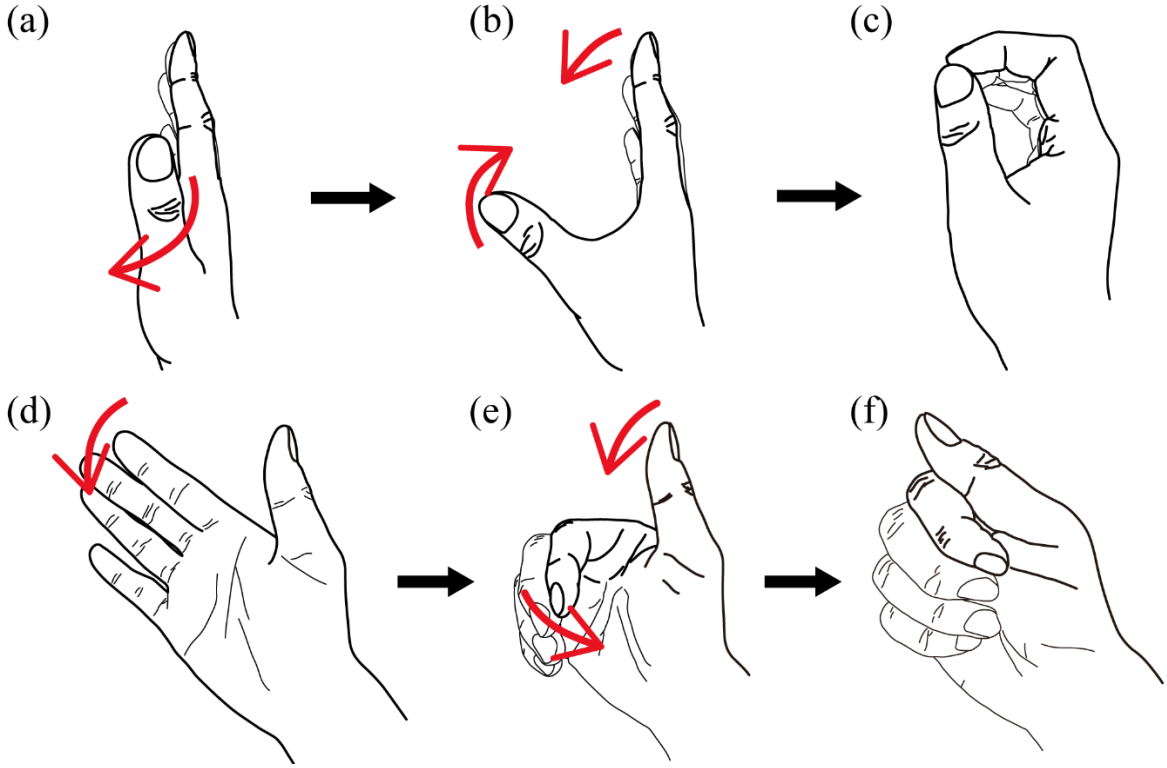

Figure. S3 Grasping strategies that are going to be realized by the system. (a)-(c) Abducted thumb grasp strategy. (d)-(f) Adducted thumb grasping strategy.

Since the mechanism pulls multiple tendons simultaneously, a predetermined grasping strategy is essential to grasp objects effectively. As grasp postures are categorized based on thumb abduction, we designed two grasping strategies (Fig. S3): abducted thumb grasping strategy (AbTGS) and adducted thumb grasping strategy (AdTGS). The sequence of required motions should be set up considering the objectives of the motions for each strategy, and the tendons should be coupled according to this sequence. For the AbTGS (Fig. S3 (a-c)), the thumb opposition starts to create a space for the object. Due to the initial posture, the space forms once the motion is complete. Once the thumb opposition is complete, the space forms between the thumb and other fingers (Fig. S3 (b)). Following this, thumb adduction and finger flexion enclose the object (Fig. S3 (c)).

When using the AdTGS to grasp the object, it is crucial to consider that the thumb can exert force on it. Initially, the space for the object is created between the index finger and thumb through index finger flexion (Fig. S3 (d)). Once the object is placed in this space, the thumb flexes to secure it, completing the grasp (Fig. S3 (f)). With the AdTGS, the object, placed on the palm, can also be grasped. This is because the index and middle fingers continue to be flexed, regardless of the thumb flexion. In both cases, the first step is the flexion of the index and middle fingers. If the object is going to be between the thumb and index finger, a lateral grasp is used to grasp the object, where the index finger is flexed to support the thumb's force. If the object is going to be between the index finger and palm, the thumb is not involved in grasping, and other fingers exert force to grasp it.

Note S4. Length-based mechanism.

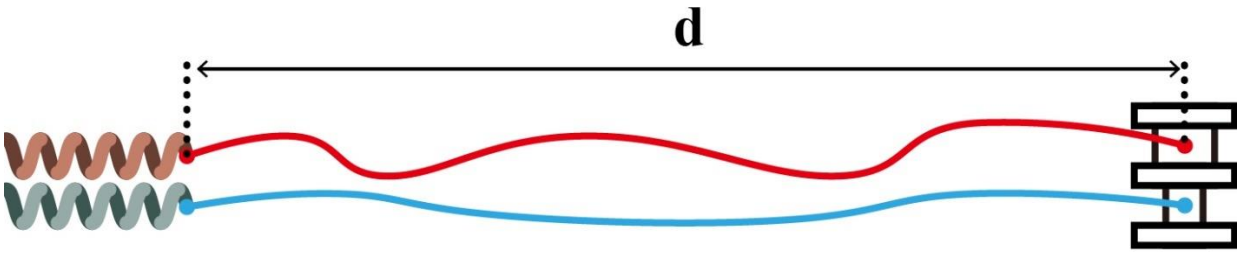

Figure. S4 Schematic of the tendon connected to the spring and the spool with different radii. d represents the distance between the end-effector and the spool.

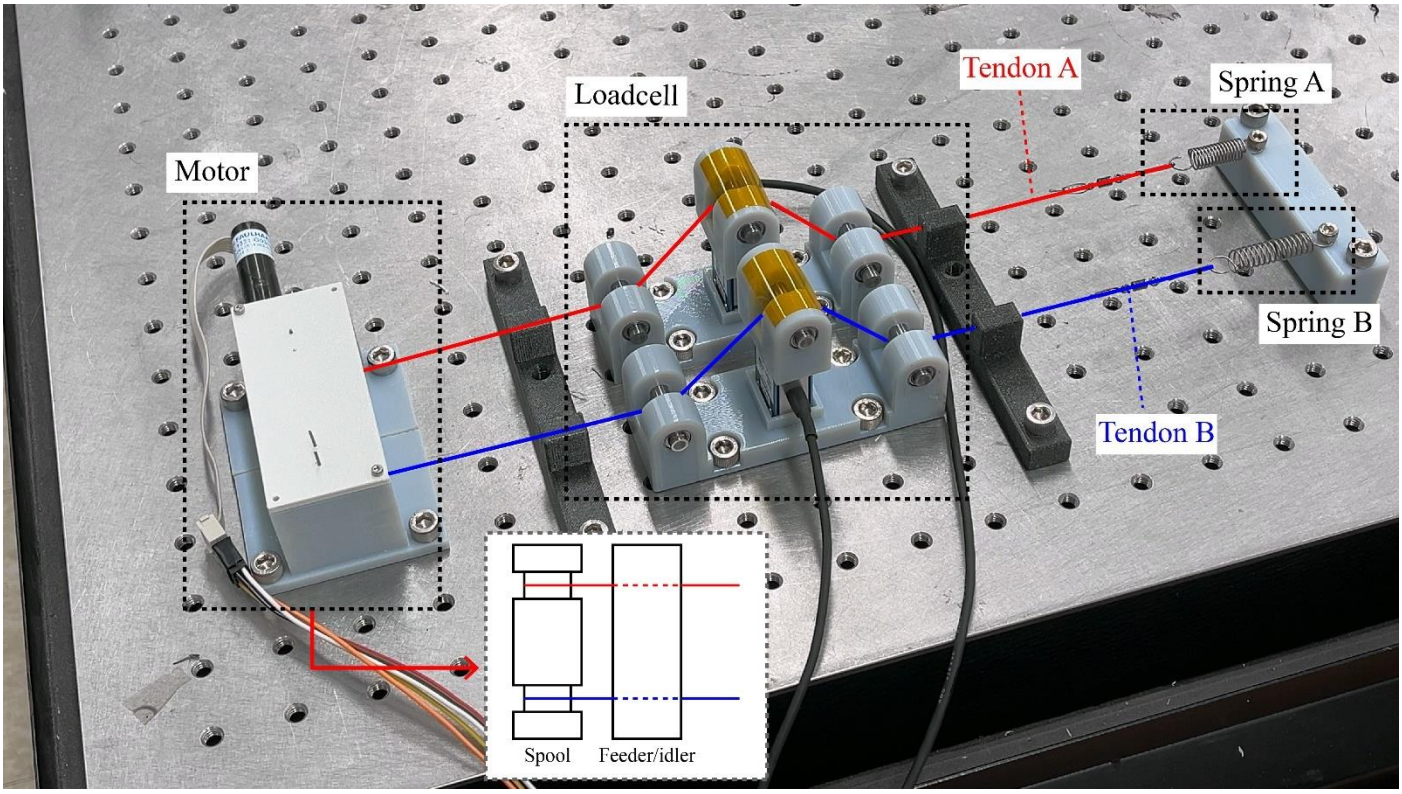

Figure. S5 Photograph of the experimental setup used to measure actuation timing differences for different spring combinations. The tendon A and the tendon B are wound on each section of the spool.

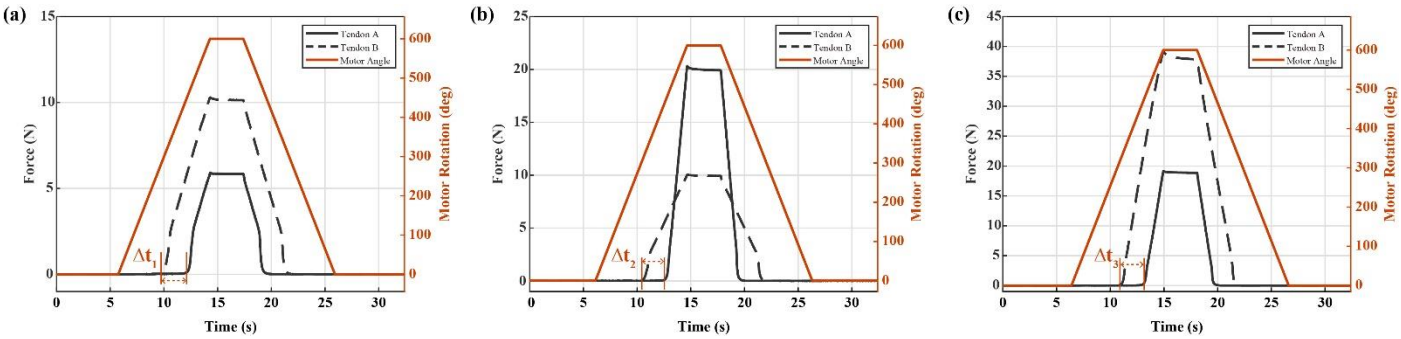

Figure. S6 Experimental result of measuring actuation timing difference test. Based on the measured tension, the timing of actuation initiation is recorded. (a) The results when the springs have the same lower stiffness (0.41N/mm). Actuation timing difference (Δt_1) was 2.175s. (b) The results when the stiffness of the spring A is 2.16N/mm and that of the spring B is 0.41N/mm. Actuation timing difference ((Δt_2) was 2.0625s. (c) The results when the springs have the same higher stiffness (2.16N/mm). Actuation timing difference ((Δt_3) was 2.15s.

Since the SSM is developed to assist finger motions, the stiffness of the finger varies depending on each finger and from person to person. Since this mechanism is based on the length of the tendon rather than the tension, the difference in stiffness of the end-effector does not affect the timing of the motion initiation. As shown in Fig. S4 and the following equations, the starting time of each actuation is determined by the length of the slack, the radii of the spool, and the angular velocity.

$$L_1 = s_1 + d \tag{1}$$

$$L_2 = s_2 + d \tag{2}$$

$$t_1 = \frac{s_1}{r_1 w} \tag{3}$$

$$t_2 = \frac{s_2}{r_2 w} \tag{4}$$

When 'i' is 1, the variables correspond to the red tendon; when 'i' is 2, the variables correspond to the blue tendon. $L_i\ (i = 1, 2)$ denotes the total length of each tendon, $s_i\ (i = 1, 2)$ denotes the slack length of the corresponding tendon, and $r_i\ (i = 1, 2)$ denotes the radius of the corresponding spool. The angular velocity of each spool, denoted as w, is the same because the tendons are wound onto different sections of a single spool.

Although the mechanism is based on the length of the tendon, we conducted an experiment to verify if the difference in tendon tension due to varying end-effector stiffness affects the mechanism. As shown in Fig. S5, a setup was implemented to test this by varying the stiffness of the springs and observing how the actuation timing differs. The experiment was conducted with three stiffness combinations using two springs: 0.41N/mm and 2.16N/mm. A hook was attached to the end of the tendon to ensure the same slack length in each experiment, and only the spring was changed, with the motor rotating by the same displacement in each trial.

The results showed that when two same springs (0.41N/mm) were used, the timing difference was 2.175 seconds; when two different springs (0.41N/mm, 2.16N/mm) were used, the difference was 2.0625 seconds; and when the other same springs (2.16N/mm) were used, the difference was 2.15 seconds (Fig. S6). The actuation start time was determined when the tension exceeded 0.1 N due to the signal noise. The timing difference was almost identical when using the same springs, with only a 0.025-second variation. This is because even with the same slack length, the minor difference in time required to surpass the 0.1 N threshold is due to the varying stiffness of the end-effector. The 0.11-second difference observed when using different types of springs can be attributed to the length difference between spring A and spring B, as these are commercial springs. The length difference between the two springs is 0.6 mm, and during the 0.11 seconds, the motor winds the tendon by approximately 0.67mm. Thus, the difference in actuation timing is not affected by the stiffness of the springs.

Note S5. Detailed design of the driving section and actuation.

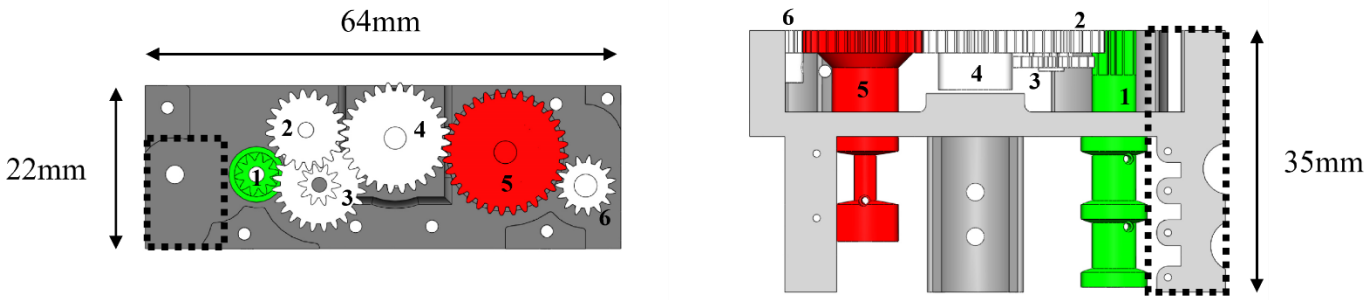

Figure. S7 Gear combination of the SSA. Gear 1: gear-embedded spool for the flexor and encloser (number of teeth: 10). Gear 2: spur gear to transmit torque from gear 4 to gear 3 (number of teeth: 20). Gear 3: compound gear to transmit torque from gear 2 to gear 1 (number of teeth: 10, 24). Gear 4: spur gear connected to the main motor (number of teeth: 28). Gear 5: gear-embedded spool for the opposer (number of teeth: 32). Gear 6: gear to enable slack-enabling for the opposer (number of teeth: 15). The dashed-line area indicates the slack-enabling mechanism section for the flexor and encloser.

The actuator was designed to maintain a minimal profile because it is mounted on a commercial armband to make the system portable. Since the device is worn on the upper arm, it was crucial to limit the height and width of the actuator, ensuring it would be lightweight and unobtrusive during daily wear. The components of the actuator (gears, spools, and slack-enabling components) are designed to fit in limited size (width: 64mm, height: 22mm, thickness: 35mm).

Angular velocity ratio:

$$w_4 : w_1 = 1 : 6.72$$

$$w_4 : w_5 = 1 : 0.875$$

$$w_5 : w_1 = 1 : 7.68$$

Tendon speed ratio

(v_1: speed of opposer, r_1: radius of the spool for the opposer = 15mm, v_2: speed of flexor, r_2: radius of the spool for the flexor and the encloser = 3mm)

$$v_1 : v_2 = r_1\, w_5 : r_2\, w_1$$

$$v_1 : v_2 = 1 : 15.36$$

With this ratio, L_1^* can be calculated through equation (5) and measured stroke length in the manuscript: $L_1^* = 55.46mm$ ($\approx 0.85\, L_1$). According to the experimental result of the AbTGS, L_1^* can be estimated through the angular displacement of the main motor and the tension of the tendon. After the thumb opposition began, the main motor rotated 1929° until the slack in the index/middle flexor was removed. Based on this, the estimated L_1^* was 44.188 mm. The difference between the two values, approximately 11 mm, is notable. This variation could be attributed to the fact that the tendon can be overlapped on the spool. Since the opposer should be released from the spool when realizing the AdTGS, some portion of the tendon remains wound on the spool even when the system is in a neutral state. This pre-wound tendon could cause overlapping of the tendon. If we assume that the tendon overlaps only once (i.e., in a single layer), the estimated value increases by approximately 10 mm. While precise measurement is challenging because tendons are connected within the SSA, considering that the tendon could be overlapped, the tendons are configured in the actuator in a desired manner.

Note S6. Self-locking mechanism in slack-length adjusting section

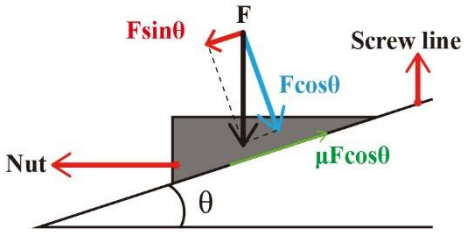

Figure S8. Freebody diagram of the screw mechanism

The nut-screw mechanism in the slack-length adjusting section allows the bolt to rotate, thereby modifying the slack length. Since the slack length should remain unchanged after it has been predetermined, the bolt and nut must form a self-locking structure. The nut and bolt create a self-locking structure if they satisfy the following equations (Fig. S8):

$$F \sin\theta \leq \mu F \cos\theta \quad (1)$$

$$\tan\theta \leq \mu \quad (2)$$

$$\tan\theta = \frac{Half\ of\ Pitch}{Diameter} \quad (3)$$

$\tan\theta\ (= 0.1)$ is lower than the previously reported friction coefficient (μ) between the PLA and the steel in dry condition [1]. This means that the slack length adjusting structure is self-locking structure.

Reference

1. P. Zhang, Z. Hu, H. Xie, G. H. Lee, and C. H. Lee, “Friction and wear characteristics of polylactic acid (PLA) for 3D printing under reciprocating sliding condition,” Industrial Lubrication and Tribology, vol. 72, no. 4, pp.533-539, 2020.

Note S7. Thumb tracking method

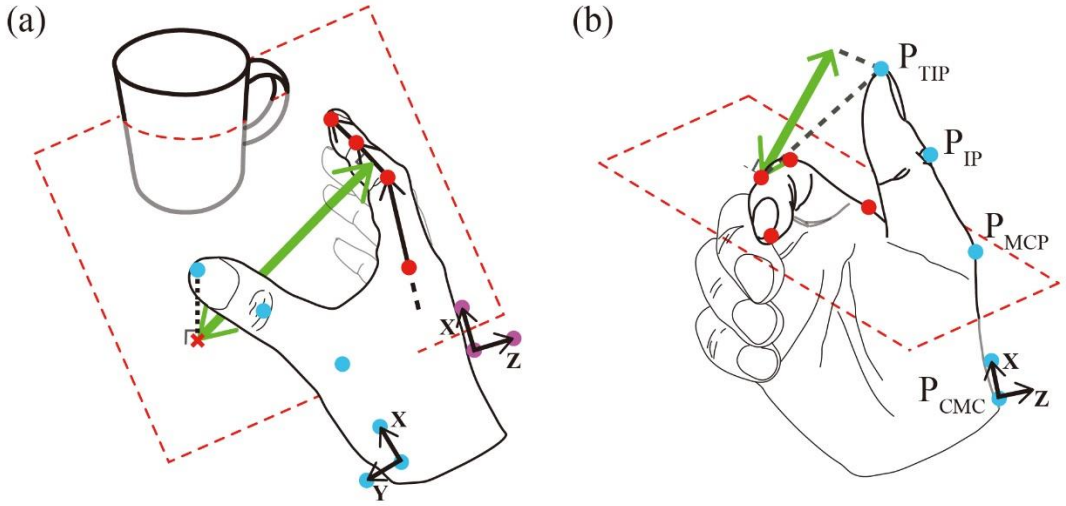

Figure. S9 Marker attachment and hand aperture size. Green arrows represent the size of the hand aperture. (a) Schematic of abducted thumb grasping strategy (b) Schematic of adducted thumb grasping strategy.

In the experiments, a motion capture system (PrimeX 13 W, Optitrack, NaturalPoint, Inc., USA) was used to track the thumb and index finger movements. As in a previous study [1], markers were attached to the thumb to calculate the joint angles (Fig. S9 (a),(b)). Similar to the method used for calculating joint angles of the CMC joint, angles of abduction and extension at the MCP joint were also calculated using the frame of the first metacarpal bone as a reference frame. Each joint angle was measured for the index finger by calculating the angle between vectors representing the corresponding bones. By adding them, the total amount of the flexion was determined.

Furthermore, the hand aperture size according to the intended grasping strategy was calculated by analyzing the correlation between markers on the index finger and the marker on the thumb tip. This is because both the AbTGS and the AdTGS (thumb-involved) anticipate an object to be positioned between the thumb and the index finger. For the AbTGS, markers of the thumb tip and the index finger were projected onto the X-Z plane of the reference frame, and the distance between the projected thumb tip marker and the projected vector representing the proximal phalanx of the index finger was calculated as the aperture size (Fig. S9 (a) green arrow). The aperture size for the AdTGS was determined by the magnitude of the vector formed by the marker on the DIP joint of the index finger and the tip of the thumb in the direction of the normal vector of the plane formed by the markers on the index finger (Fig. S9 (b) green arrow).

Reference

1. D. H. Kim, Y. Lee, and H.-S. Park, “Bioinspired high-degrees of freedom soft robotic glove for restoring versatile and comfortable manipulation,” Soft robotics, vol. 9, no. 4, pp. 734–744, 2022.

Note S8.

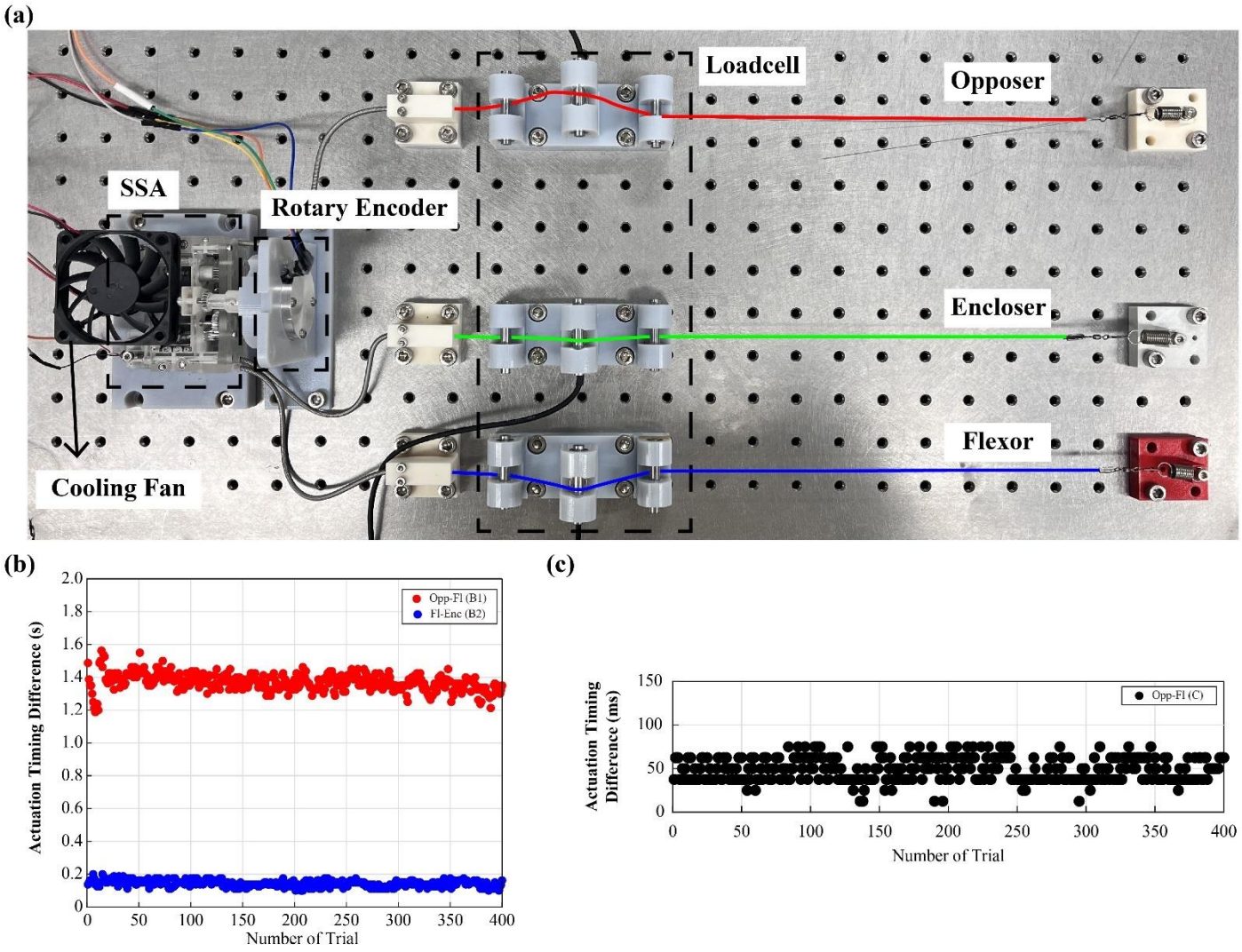

Figure. S10 Experimental setup and results of testing the robustness of the system. (a) The experimental setup for the robustness test. (b) Actuation timing differences during the SSA actuation for the AbTGS. "Opp-Fl" (red dots) represents the actuation timing difference between the opposer and the flexor. "Fl-Enc" (blue dots) represents the timing difference between the flexor and the encloser. (c) Actuation timing difference between the flexor and the encloser during SSA actuation for the AdTGS.

An experimental setup was designed to test the system's robustness by simulating the actuation scenario. The SSA was modified to use springs as the end-effectors instead of the glove for repeated experiments (Fig. S10(a)). The tendons, labeled as opposer, encloser, and flexor, were tied to spools in each section, same as in the actual scenario (Fig. 5 in the manuscript). Using spring sheaths as Bowden cables, tendons from the actuator pass through a tension measuring device. The SSA's mechanism and structure are the same as those of the EGP3, but the main motor was replaced to enable faster repetitions. An external rotary encoder was attached to measure rotational displacement. The experiment was repeated 400 times, with each cycle consisting of a 127° counterclockwise motor rotation (AbTGS), returning to the starting point, a 100° clockwise rotation (AdTGS), and then returning to the starting position. As described in Note S4, actuation was defined as starting when the tension exceeded 0.1 N.

Graphs show how the actuation timing differences varied when driven in counterclockwise and clockwise directions, simulating AbTGS and AdTGS, respectively (Fig. S10(b-c)). Figure S10(b) shows the timing difference between the opposer and flexor and between the flexor and encloser when the motor rotated in reverse to implement the AbTGS. The average actuation timing difference between the opposer and flexor (B1) was 1.3673s, with a standard deviation of 0.0538s. The timing difference between the flexor and encloser (B2) averaged 0.1428s, with a standard deviation of 0.0193s. While both B1 and B2 maintained timing

differences within a consistent range, B1 shows more variability than B2. This is likely because the spool for the opposer has a small diameter (3mm), which causes the tendon to be wound inconsistently due to the bending stiffness of the tendon. Adding a groove to the spool, similar to a screw, is expected to help the tendon to be wound consistently and further reduce variability in actuation timing differences [1].

Fig. S10(c) shows that the timing difference between the flexor and encloser (C) was also consistent when actuated during the AdTGS. The average timing difference for C was 0.0488 seconds, with a standard deviation of 0.0134 seconds. Despite having the same slack length difference as B2, the timing difference of C is shorter. This is because, in the case of B2, the tension of the opposer already applies a load to the main motor, causing the angular velocity of the motor speed for B2 to be slower (by approximately 2.5 times).

Reference

1. P. Tran, S. Jeong, S. L. Wolf, and J. P. Desai, “Patient-specific, voice-controlled, robotic flexotendon glove-ii system for spinal cord injury,” IEEE Robotics and Automation Letters, vol. 5, no. 2, pp. 898–905, 2020.

Note S9. Grip strength measurement

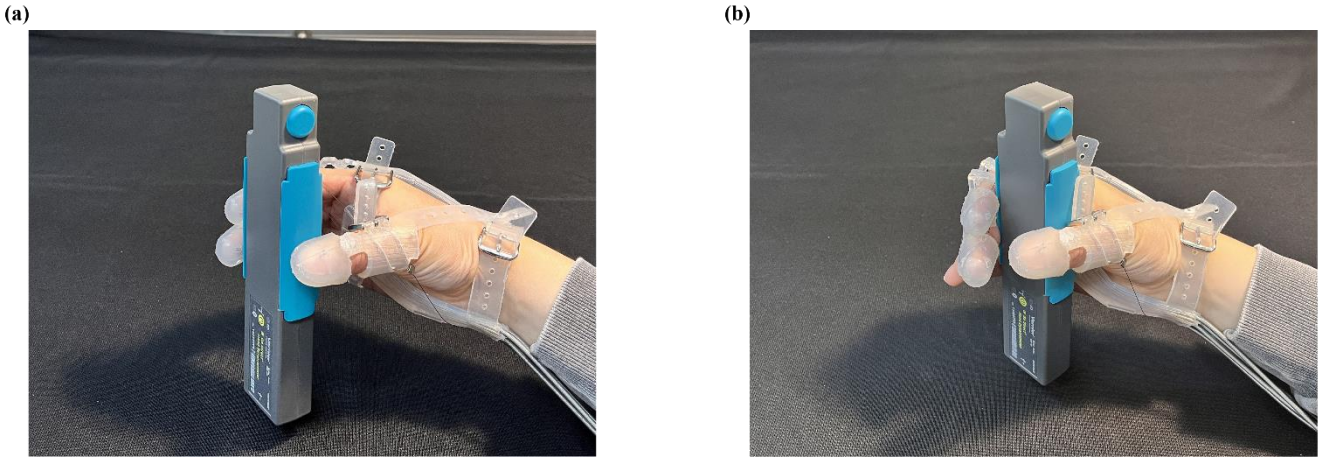

Figure. S11 Two scenarios of measuring grip strength using the AbTGS. The object is a digital dynamometer. (a) Gripping with the fingertips. (b) Holding the object inside the hand.

Figure. S12 Experiment setup using a pressure pad. (a) Measurement devices. Blue pad: pressure pad. Yellow object: 3D printed flat object (5mm thickness) for the lateral pinch experiment. Red object: 3D printed cylindrical object (diameter: 60mm) for the wrap grasp.

Table S1. Measured grip strength using a dynamometer. The grip strength of the fingertips and wrap grasp is measured with both EGP II and EGP III.

	Gripping with fingertips (N)	**Wrap grasp (N)**
EGP II	8.1	8.6
EGP III	5.6	8.3

Table S2. Measured force applied to the object using a pressure pad. The grasp force of the wrap grasp and the lateral pinch is measured using EGP II and EGP III. Since the EGP II cannot grasp objects with the lateral pinch, only wrap grasp performance was measured.

	Wrap grasp (N)	**Lateral pinch (N)**
EGP II	20.2	-
EGP III	15.4	5.6

We used a digital dynamometer (Go Direct Hand Dynamometer; Vernier) and a pressure pad (Pliance; novel electronics inc.) to measure the grip strength of the system. The digital dynamometer was used to measure the grip strength of the fingertips and wrap grasp while performing the AbTGS (Fig. S11). Since the dynamometer measures the force perpendicular to the surface of the measurement area, the grip strength of the wrap grasp was also measured by the pressure pad to measure the total force applied to the object (as conducted in [1], Fig. S12(b)). Furthermore, the force applied to the flat object by the lateral pinch was

measured by the pressure pad (Fig. S12(c)). Measurements were conducted three times for each case, and the measured force was averaged. To compare with the previous version of the system, grip strength was also measured for the EGP II. Since the EGP II is also capable of wrap grasp and grasping objects with fingertips, the dynamometer and pressure pad were used to measure its performance, respectively.

The grip strength is not only related to the mechanism used but also heavily influenced by the motor employed during actuation. To ensure a fair comparison between the EGP II and EGP III, grip strength was measured using the same actuator. For the EGP III, grip strength was measured with the opposer, encloser, and flexor all engaged, realizing each grasping strategy. For the EGP II, the opposer and encloser were removed from the EGP III, and only the flexor was actuated by the main motor. Since EGP II utilizes an active extension, the passive extensor in EGP III was also removed for measurement.

The grip strength was measured for two scenarios using a dynamometer: when gripping with the fingertips (Fig. S11 (a)) and when an object was held inside the hand (wrap grasp, Fig. S11(b)). For the first scenario, the grip strength of the EGP II was higher than that of the EGP III. This is because the motor pulls three tendons simultaneously in the EGP III, and the thumb encloser participated less in the grasping due to the thickness of the dynamometer. For the second scenario, since the dynamometer was held inside the hand, the force applied to the dynamometer by the proximal parts of the fingers was measured. In this case, the EGP II and the EGP III showed similar grip strength levels for the wrap grasp (Table S1). Compared to gripping with fingertips, the index and middle fingers and the thumb wrap the dynamometer so that the encloser participates in grasping more.

To measure the total normal force applied to the object while performing the wrap grasp, a 3D-printed cylindrical object (diameter: 60mm) wrapped by the pressure pad was used (Fig. S12(a)). Similar to the grip strength measured by the dynamometer, the total force exerted on the object was greater for the EGP II (Table S2). However, considering the previously reported wrap grasp performance of the EGP II (maximum of 10.6 N when using a cylindrical object with a diameter of 50 mm [1]), the performance of the EGP III is acceptable.

To measure grip strength using the pressure pad, the pad was placed on a 3D-printed flat object (5 mm thickness, Fig. S12(a)). The pressure pad and the object were placed between the index finger and the thumb. While realizing the AdTGS, the thumb applied force to the pad, and the force was recorded as 5.6N (Table S1).

The experiments validated that the EGP III could exert sufficient force on the object, comparable to the EGP II.

Reference

1. B. B. Kang, H. Choi, H. Lee, and K.-J. Cho, “Exo-glove poly ii: A polymer-based soft wearable robot for the hand with a tendon-driven actuation system,” Soft robotics, vol. 6, no. 2, pp. 214–227, 2019.

Note S10. Motion generation with the slack-based sequential actuator when length of all slack is zero.

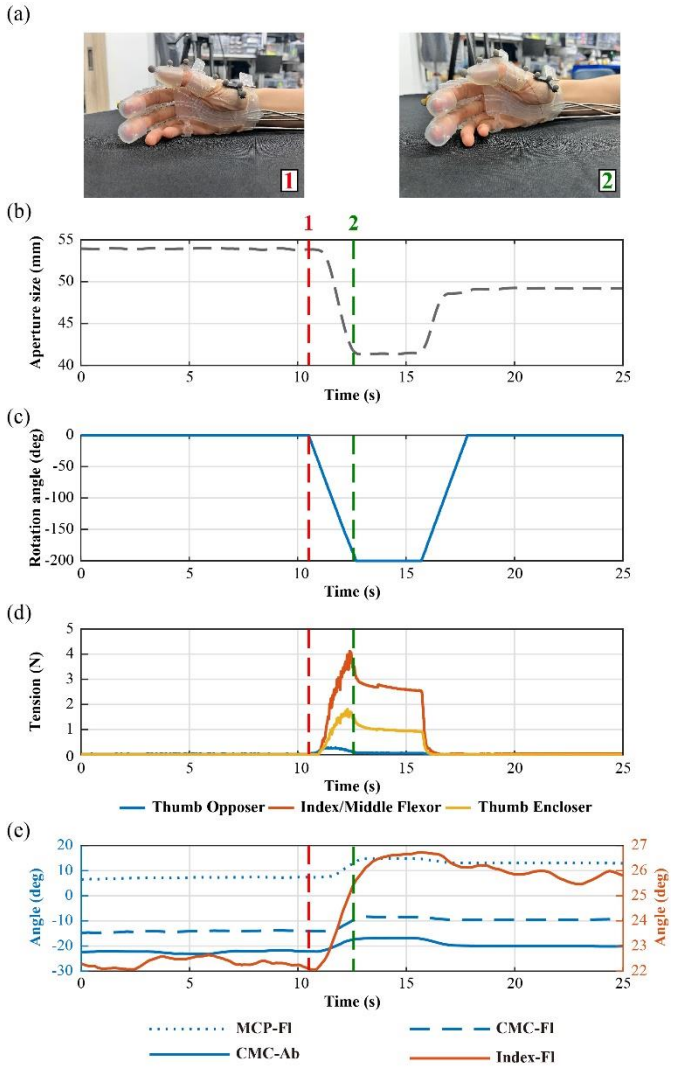

Figure. S13 Experimental results of motion generation with the SSA when all slack lengths are zero. (a) Photograph of the hand posture at two different time frames. The number and color of each label in the photo correspond to the number and the color of the dashed line in the graph. (b) Hand aperture size according to the time. Since the flexion of the index and middle fingers is not generated, the line is shown in gray and marked with a dashed style. (c) Angle spanned by the motor. The angle of rotation is a negative value because the motor rotates counterclockwise. (d) Tension of tendons. (e) Measured joint angle during the experiment. Fl and Ab denote flexion and abduction, respectively.

We set the slack length of each tendon to zero. With no slack in the tendons, the fingers (including the thumb) were pulled simultaneously at different speeds for each tendon. The main motor rotated counterclockwise to pull all tendons, continuing until the thumb made contact with the index finger. However, the tension of the opposer increased to 0.27N and decreased to zero. This occurred because the thumb encloser was pulling simultaneously, reducing the distance between the pulley location of the thumb opposer and its insertion point. As a result, no movement occurred due to the thumb opposer.

As shown in Fig. S13(e), the thumb abducts, but this is not caused by the opposer; instead, it results from the encloser's pulley being positioned closer to the palm, which pulls the thumb to be abducted. Since the intended grasping strategy was not achieved, the hand aperture was not properly formed, as indicated by the gray dashed line in Fig. S13(b). Fig. S13(a) shows the hand posture at corresponding timing, with minimal movement (MCP flexion: about 7.5 degrees, CMC flexion: about 6 degrees, and index flexion: 4.3 degrees). Compared to the pre-programmed slack lengths for each tendon (Fig. 8-9 in the manuscript), we found that although the tendons were pulled at different speeds, the intended grasping strategy could not be realized without setting appropriate relative slack length.

Note S11. Achievable common grasps used in daily living.

Vergara et al. reported about common grasps used by adults during daily living [1]. In the study, the authors categorized grasp postures into nine postures: cylindrical grasp (Cyl), oblique palmar grasp (Obl), hook grasp (Hook), lumbrical grasp (Lum), intermediate power-precision grasp (IntPP), pinch grasp (Pinch), lateral pinch (LatP), special pinch (SpP), and non-prehensile grasp (NonP). Given that, we tried to grasp objects with the categorized postures except the NonP because NonP is a posture for manipulating the objects without grasping. Among the postures, 87.5% (7/8) were successfully achieved. Since the flexor pulls both index and middle fingers simultaneously with the differential mechanism, the IntPP was challenging to realize (especially the photograph of the posture in the categorization [1]).

Although the EGP III can achieve 87.5% of common grasps, real-world objects are designed for bare hands (without wearable hand robots). This means that since the hand equipped with the EGP III is bulkier than a bare hand, some objects with limited space for grasping cannot be grasped. Designing a robot with a slimmer profile would likely expand its grasping capabilities.

Reference

1. M. Vergara, J.L. Sancho-Bru, V. Gracia-Ibáñez, and A. Pérez-González, “An introductory study of common grasps used by adults during performance of activities of daily living,” Journal of Hand Therapy, vol. 27, no. 3, pp.225-234, 2014.